ACTUATORS

A soft ring oscillator

Daniel J. Preston[1,2], Haihui Joy Jiang[1,3], Vanessa Sanchez[1,2,4], Philipp Rothemund[1,4,5], Jeff Rawson[1], Markus P. Nemitz[1,2], Won-Kyu Lee[1], Zhigang Suo[4,5], Conor J. Walsh[2,4], George M. Whitesides[1,2,5]*

Periodic actuation of multiple soft, pneumatic actuators requires coordinated function of multiple, separate components. This work demonstrates a soft, pneumatic ring oscillator that induces temporally coordinated periodic motion in soft actuators using a single, constant-pressure source, without hard valves or electronic controls. The fundamental unit of this ring oscillator is a soft, pneumatic inverter (an inverting Schmitt trigger) that switches between its two states ("on" and "off") using two instabilities in elastomeric structures: buckling of internal tubing and snap-through of a hemispherical membrane. An odd number of these inverters connected in a loop produces the same number of periodically oscillating outputs, resulting from a third, system-level instability; the frequency of oscillation depends on three system parameters that can be adjusted. These oscillatory output pressures enable several applications, including undulating and rolling motions in soft robots, size-based particle separation, pneumatic mechanotherapy, and metering of fluids. The soft ring oscillator eliminates the need for hard valves and electronic controls in these applications.

INTRODUCTION

Soft actuators and robots can simplify certain mechanical tasks, such as grasping, using their inherent "material intelligence" (*1*–*3*). Soft devices may, however, rely on hard, electronic control systems, and completely soft devices remain constrained in their capabilities. Specifically, periodic pneumatic actuation of multiple components has relied on hard valves and electronic control. This work describes a completely soft ring oscillator, composed of an odd number of soft, pneumatic inverters. This soft ring oscillator generates multiple oscillating, temporally offset output pressures from one constant input pressure; these output pressures can, in turn, drive soft actuators and robots without the need for hard valves or electronic controls.

Soft devices offer several useful characteristics, including (i) collaboration (safety and compatibility with humans and animals) (*1*, *3*), (ii) the ability to conform to their surroundings and to objects with which they interact (*1*), (iii) simplicity and low cost (*1*), (iv) ease of sterilization for medical and food applications (*4*), (v) high cycle lifetime (*5*–*7*), and (vi) resistance to damage by impact (*1*, *3*). Fluid-driven soft actuators function by pressurizing elastomeric channels and chambers whose geometry is designed to direct motion, but each actuator usually requires hard valves and electronic components for control (typically hard solenoid valves that open and close in response to electronic signals) (*2*, *3*, *8*–*13*). Actuation schemes include both external hard valves with pneumatic tethering (*8*, *9*) and internal hard valves that avoid tethering but result in devices that are not completely soft (*13*, *14*). Temporally coordinated oscillation of multiple sources of pressure, in particular, has required many hard valves in previous work (*11*, *12*, *15*). Basic soft valves have begun to be incorporated directly into soft devices—e.g., unidirectional check valves have enabled simple control of gas flow in a soft "jumper" powered by combustion (*16*), and microscale valves periodically inflated and deflated the arms of a soft, octopus-shaped structure (*17*)—but the scope of these applications is small. More recent work has enabled temporally coordinated actuation of multiple components using a single pneumatic on/off signal by taking advantage of the fluidic resistance between components (*18*, *19*), but control of this on/off signal still requires hard infrastructure, and cyclic or repeated actuation requires continuous control.

Microfluidic devices have been designed as controllers, timers, and oscillators (*20*–*22*), including pneumatic ring oscillators (*21*, *22*), but two issues have limited their adoption in soft robotics. First, most applications of soft pneumatic devices involve macroscopic motions and require substantial volumes of gas, and the microfluidic systems that have been examined are usually not useful in these applications because flow rates through them are low (because of large pressure drops in small internal channels). For example, in recent work in which soft actuators were driven by a microfluidic controller (*17*), the microfluidic controller achieved, at its most rapid, a period of about 50 s between actuations. Second, microfluidic devices have typically relied on components fabricated in hard materials (glass or hard plastics), thus limiting their compatibility with, and integration within, entirely soft devices (*20*–*24*). Most soft microfluidic devices—based on valve designs proposed by Quake and coworkers (*25*) and by Hosokawa and Maeda (*26*) and later expanded upon by the groups of Mathies (*27*, *28*) and Hui (*22*, *24*)—have been limited to polydimethylsiloxane (*25*, *26*, *29*) and have required external, electronic control, with some exceptions not relying on either hard materials or electronic controls (*17*, *21*). Oscillators based on soft dielectric elastomers have also relied on hard plastic components for support (*30*, *31*).

As a step toward enabling control and actuation within entirely soft devices, we developed a macroscopic soft valve (configured here as a pneumatic inverting Schmitt trigger—a type of operational amplifier) that uses a pressure signal to switch between two states (each state corresponding to the occlusion of one of the two internal pathways for airflow within the valve) (*5*). This valve can amplify pressure, filter noise, allow autonomous interaction of devices with their environment, and oscillate between its two states (*5*); by itself, it cannot, however, generate multiple, temporally coordinated oscillating output pressures for movements such as rolling, slithering, or swallowing.

Here, we harness three instabilities—buckling of tubes to form kinks that prevent the flow of air, snap-through of a hemispherical

[1]Department of Chemistry and Chemical Biology, Harvard University, 12 Oxford St., Cambridge, MA 02138, USA. [2]Wyss Institute for Biologically Inspired Engineering, 3 Blackfan Circle, Boston, MA 02115, USA. [3]School of Chemistry and Sydney Nano Institute, University of Sydney, Sydney, NSW 2006, Australia. [4]John A. Paulson School of Engineering and Applied Sciences, Harvard University, 29 Oxford St., Cambridge, MA 02138, USA. [5]Kavli Institute for Bionano Science and Technology, Harvard University, 29 Oxford St., Cambridge, MA 02138, USA.
*Corresponding author. Email: gwhitesides@gmwgroup.harvard.edu

membrane, and the systematic instability created when an odd number of inverters are connected to each other in a loop—to enable an entirely soft, pneumatic ring oscillator that uses a single input at constant pressure to generate multiple periodic, temporally coordinated output pressures (Fig. 1A). This ring oscillator relies on three soft, pneumatic inverters (*32*, *33*); we connected an odd number of these inverters in a ring, resulting in autonomous and sequential oscillation between high- and low-pressure states (because this system, when comprising an odd number of inverters, has no stable configuration) (Fig. 1B). The frequency of the soft ring oscillator depends on three parameters: (i) the value of the constant input pressure, (ii) the resistance to airflow of the connections between inverters, and (iii) the volumes of gas required to actuate the components attached to the ring oscillator (i.e., pneumatic capacitance). To understand the ring oscillator better and to enable the design of future systems, we developed an analytical model for the oscillation frequency as a function of these parameters. We also demonstrated the use of the ring oscillator in five prototypical applications, each composed entirely of soft components and driven by only a single, constant-pressure input: (i) transporting an object on an undulating track, (ii) sequentially inflating actuators that caused a soft robot to translate by rolling, (iii) sorting solid particles by size, (iv) actuating a textile-based mechanotherapeutic device applied to the (human) lower leg, and (v) metering known doses of fluids in a repeating pattern.

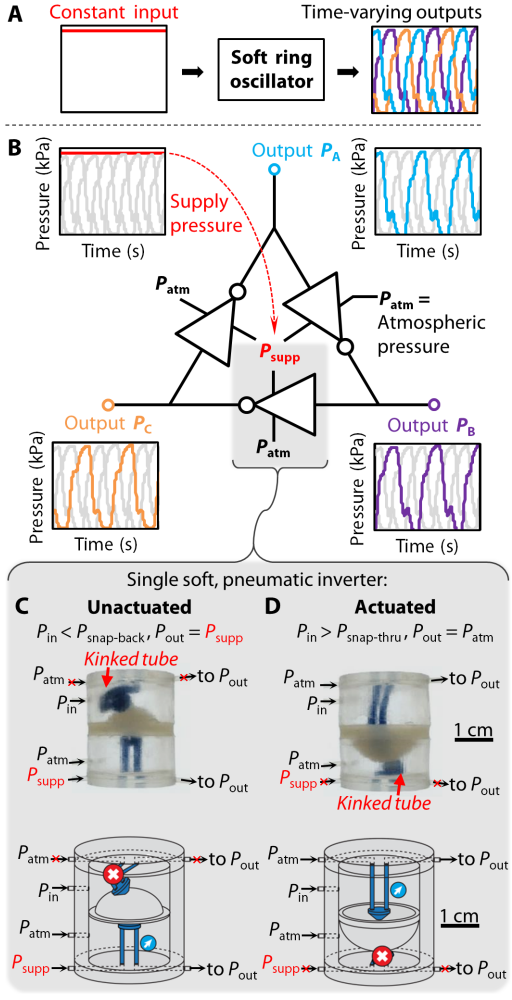

Fig. 1. The soft ring oscillator composed of three elastomeric, pneumatic inverters. (**A**) The soft ring oscillator converts a constant input pressure to multiple temporally coordinated oscillating outputs. (**B**) The ring oscillator is composed of three inverters connected in a loop, resulting in a systematic instability (because no stable state exists); it is driven by a constant supply pressure, P_{supp}, and generates output pressures P_A, P_B, and P_C. Side views of a single soft inverter show the internal tubes for airflow, with the upper tube kinked by the membrane in (**C**) and the lower tube kinked in (**D**) (top, photo; bottom, schematic; 2D schematic shown in fig. S8). The output pressure, P_{out}, is an inverted signal of the input pressure, P_{in}, with hysteresis due to the difference in the pressures required to snap the membrane from its initial state ($P_{snap\text{-}thru}$) and allow the membrane to return back to its initial state ($P_{snap\text{-}back}$); this behavior exemplifies an inverting Schmitt trigger (detailed characterization in fig. S11 and operation shown in movie S1).

RESULTS

The soft, pneumatic inverter

The soft, pneumatic inverter used here is an elastomeric valve with two states. When configured with inputs and outputs connected as shown in Fig. 1C, the inverter behaves as an inverting Schmitt trigger (*32*, *33*): The output pressure decreases to a low value when the input pressure rises above a given threshold, and the output pressure increases to a high value only when the input pressure falls below a different, smaller threshold (detailed in fig. S11), i.e., it is an inverting switch characterized by hysteresis. Our pneumatic inverter is distinct, however, from electronic transistors [and their microfluidic equivalent, Quake-type valves (*25*)] in that transistors only open or close one pathway for flow. To create an inverter, a pull-up or pull-down resistor is required to achieve a second output state (when the transistor does not allow flow). In contrast, our soft pneumatic inverter opens and closes two pathways for flow simultaneously, eliminating the need for an added resistor and, consequently, resulting in a more energy-efficient inverter that only requires power to switch but does not require power at steady state. This enhanced efficiency is realized during inflation of actuators using the ring oscillator, where one inverter allows airflow to an actuator until it is pressurized and the other dormant inverters do not draw any power (airflow), in contrast to previously described microfluidic approaches in which even the dormant oscillators must draw power (airflow), resulting in wasted energy.

The inverter is composed of two elastomeric, cylindrical chambers separated by a hemispherical elastomeric membrane (Fig. 1, C and D, with pneumatic connections detailed schematically in fig. S8). The bottom chamber is connected to atmospheric pressure, P_{atm} = 0 kPa (gauge pressure), and the top chamber is connected to a variable input pressure, P_{in}. Because of the constraints imposed by the cylindrical walls, the membrane initially decreases in area (i.e., compresses) and then later increases in area, as it transitions from its initial unactuated state inside of the upper chamber of the inverter to its actuated state in the lower chamber; this behavior leads to an instability (*34*), which causes the membrane to "snap" to its actuated state in the bottom chamber when the pressure in the top chamber reaches a critical pressure, $P_{snap\text{-}thru}$, and to snap back to its unactuated state when the pressure in the top chamber decreases below a critical pressure, $P_{snap\text{-}back}$ (fig. S9; the hysteresis is due to the characteristic of the inverter that $P_{snap\text{-}back} < P_{snap\text{-}thru}$).

Elastomeric tubing passes through both chambers (fig. S2). This tubing can be kinked by the internal hemispherical membrane depending on the direction in which the membrane deflects (exhibiting a second, distinct form of instability, i.e., buckling of the internal

tubes to form kinks). The upper tubing is kinked by the membrane in the unactuated state (when P_{in} is low, i.e., $P_{in} < P_{snap\text{-}back}$) and allows P_{out} to connect only to P_{supp} through the lower tubing (Fig. 1C). Meanwhile, in the actuated state (when P_{in} is high, i.e., $P_{in} > P_{snap\text{-}thru}$), the lower tubing is kinked by the membrane and allows P_{out} to connect only to P_{atm} through the upper tubing (Fig. 1D), effectively inverting the input signal (movie S1). The snap-through and snap-back pressures ($P_{snap\text{-}thru}$ and $P_{snap\text{-}back}$, respectively) do not depend on the supply pressure (fig. S12).

The soft ring oscillator

We designed the soft, pneumatic ring oscillator with three inverters connected in a loop (Fig. 1B). Multiple inverters connected in series (i.e., the output pressure P_{out} of one inverter acts as the input pressure P_{in} of the next inverter) will take alternatingly unactuated ($P_{out} = P_{supp}$) and actuated ($P_{out} = P_{atm}$) states in a stable configuration. To create the "ring," we connected the output from the last inverter in the series to the input of the first inverter; no stable state exists for this system of three inverters (or for any odd number of inverters), and an instability travels along the ring as inverters sequentially inflate and deflate (Fig. 2, A and B, and movie S2). This propagating instability leads to periodic, temporally offset oscillation of the output pressures ($P_{out} = P_A$, P_B, and P_C) (Fig. 2C), each shifted by 120° in phase. We fabricated the ring oscillator with three indistinguishable inverters, made primarily from the commercially available elastomer Dragon Skin 10 NV ($P_{snap\text{-}thru}$, ~11 kPa; $P_{snap\text{-}back}$, ~2.5 kPa) (see Materials and Methods for fabrication and characterization), and connected it to a supply of compressed air at constant pressure (P_{supp} = 17 kPa). After an initial transient state of ~1 s, during which all three inverters began to inflate, an instability formed spontaneously and traveled around the ring, generating a periodic oscillation of the output pressures of each inverter (oscillation period = 3.1 s, calculated from the average peak-to-peak distance in the plot of pressure versus time at one of the three outputs; Fig. 2C). Because of the pneumatic capacitance C (in kg/Pa) due to the internal air volume of the system (Fig. 3A) and the flow resistance R (in Pa-s/kg) of the tubing inside and in between inverters (Fig. 3A), the output pressures of the inverters did not instantaneously switch between P_{atm} and P_{supp} but rather required some time to change (in this case, for each inverter, inflation time was $t_i \approx 0.35$ s and deflation time was $t_d \approx 0.65$ s).

We also explored the limits of the soft ring oscillator. First, we slowly increased the supply pressure to a ring oscillator (at a rate of less than 1 kPa/s) until failure, which occurred at a supply pressure of 44 kPa because of disconnection of the tubing attached to one of the inverters. Second, with a constant supply pressure of 17 kPa, we allowed the ring oscillator to cycle continuously for more than 15,000 complete periods; during this cycling test, we did not observe any change in frequency or degradation in performance. Last, while the ring oscillator was operating, we mechanically deformed it by manually compressing all three of the inverters to more than 75% compressive strain; after releasing the compressive force, the ring oscillator resumed operation immediately (movie S2).

Analytical model for the soft ring oscillator

We characterized the dependence of the period of oscillation of the ring oscillator on each of three adjustable system parameters: the supply pressure, the pneumatic resistance, and the pneumatic capacitance. The ring oscillator can be understood through an analogous electrical circuit (Fig. 3A), where each inflation or deflation event (Fig. 2, A and B, detailed in fig. S13) can be modeled as charging or discharging of the corresponding components in a resistor-capacitor (RC) circuit. We first varied supply pressure, P_{supp}, from 11 kPa (= $P_{snap\text{-}thru}$) to 20 kPa (Fig. 3B). For $P_{supp} < 11$ kPa, the inverters do not reach the critical pressure required for the internal membrane to snap through, so we did not observe oscillations. The oscillation period decreased monotonically with increasing supply pressure because the inverters inflated more rapidly, whereas deflation time remained constant (Fig. 3B).

When integrated into a soft robot, additional tubing between inverters increases resistance to airflow, R (in Pa-s/kg), and the volume of the attached actuators to be driven by the ring oscillator increases the pneumatic capacitance, C (in kg/Pa). To investigate the influence of additional resistance on the oscillation period, we added tubing with an inner diameter of 0.97 mm and lengths ranging from 0 to 1.27 m, with pneumatic resistance R_{tube}, between each of the inverters in the ring oscillator (fig. S13 and eq. S1). The oscillation period increased linearly with the length of the tubing (Fig. 3C). We simulated actuators by attaching glass jars, each with identical pneumatic capacitance C_{res}, between each inverter (fig. S13 and eq. S2). We varied

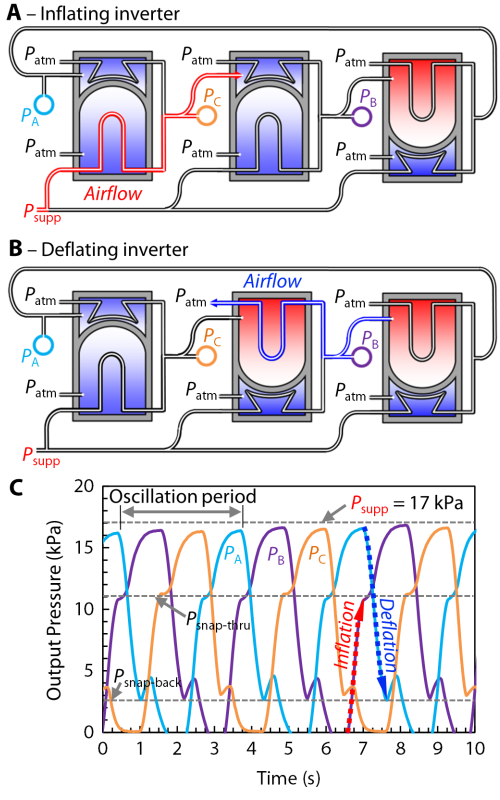

Fig. 2. The two states of the ring oscillator: Inflation and deflation. The ring oscillator always contains either two adjacent unactuated inverters (**A**), in which case one of the inverters inflates, or two adjacent actuated inverters (**B**), in which case one of the inverters deflates. (**C**) The three-inverter ring oscillator generates three temporally coordinated output pressures, shown here as P_A, P_B, and P_C, when a constant supply pressure, P_{supp}, is applied. Horizontal dashed gray lines indicate the supply pressure, P_{supp}; the snap-through pressure required to transition the internal membrane from its unactuated to its actuated state, $P_{snap\text{-}thru}$; and the snap-back pressure beneath which the internal membrane transitions from its actuated to its unactuated state, $P_{snap\text{-}back}$. The red and blue dashed arrows overlaid onto the plot indicate inflation and deflation, respectively.

the air volume inside of the glass jars (and therefore the pneumatic capacitance C_{res}) from 0 to 315 ml by partially filling them with water, and the oscillation period increased linearly with the air volume of these capacitors (Fig. 3D).

To derive an equation for the dependence of the oscillation period as a function of the pneumatic capacitance C, the flow resistance R, the supply pressure P_{supp}, and the number of inverters in the ring n, we modeled the airflow between two adjacent inverters that are in the same state of actuation (which is where the instability occurs), during both inflation and deflation (fig. S13), and extended the result to the entire ring oscillator. The oscillation period of a ring oscillator containing n inverters is therefore the sum of the rise times and fall times, corresponding to inflation and deflation, respectively, of all n inverters (Eq. 1, with derivation in the Supplementary Materials)

$$t_{period} = n\,R\,C\left[\ln\left(\frac{P_{atm}-P_{supp}}{P_{snap\text{-}thru}-P_{supp}}\right)+\ln\left(\frac{P_{supp}-P_{atm}}{P_{snap\text{-}back}-P_{atm}}\right)\right] \quad (1)$$

The model prediction was plotted, along with experimentally measured data recorded during operation of the ring oscillator, in Fig. 3, B to D; the model showed good agreement with the experimental data, suggesting that it may therefore be used as an analytical tool to either predict system performance for, or guide future application-specific designs of, the soft ring oscillator.

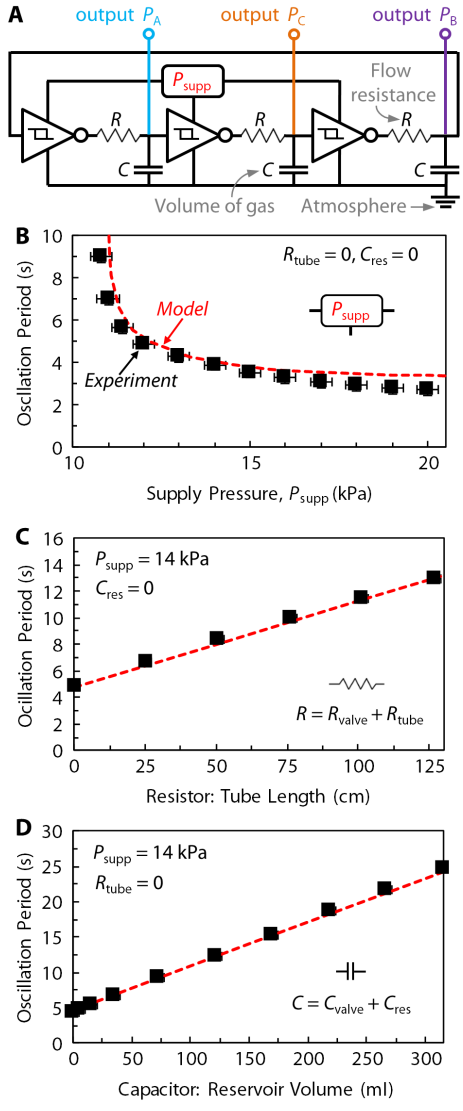

Fig. 3. Response to variable supply pressure, pneumatic resistance, and pneumatic capacitance. (**A**) A constant supply pressure, P_{supp}, drives the system, which exhibits resistances and capacitances due to friction during airflow and pressurization of volumes of gas, respectively. We performed experimental parametric sweeps over multiple supply pressures (**B**), pneumatic resistances resulting from thin-diameter tubing added between inverters (**C**), and pneumatic capacitances provided by added volumes of gas (**D**). Error bars represent 95% confidence intervals of the means. (B to D) Predictions from the analytical RC circuit model are overlaid as dashed red curves.

Applications of the soft ring oscillator

We demonstrated the ability of the ring oscillator to drive motion, using only a single, constant input pressure, in two applications: translating a ball around a track (Fig. 4) and driving a rolling soft robot (Fig. 5). The track for ball translation consists of a row of chambers connected to the outputs of the ring oscillator (i.e., P_A, P_B, and P_C) in a repeating pattern; the ring oscillator sequentially inflates these chambers and pushes the ball forward (Fig. 4A). Changing the order of the

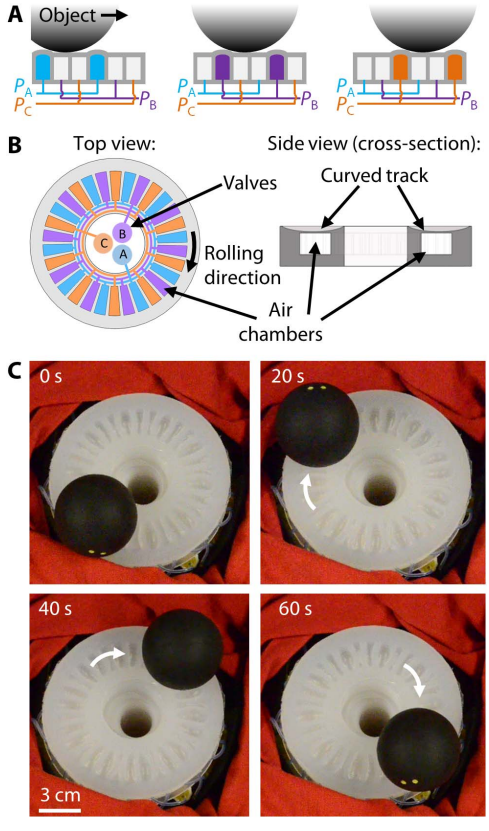

Fig. 4. Translation of a spherical object. The soft ring oscillator rolls a ball on an elastomeric track. The track relies on sequential inflation of serially arranged elastomeric chambers to translate objects (**A**). A circular track can roll a ball indefinitely; the schematic illustrates a completely soft design of a circular track with 30 internal chambers (**B**), which we used in an experimental demonstration shown here (**C**) and in movie S3.

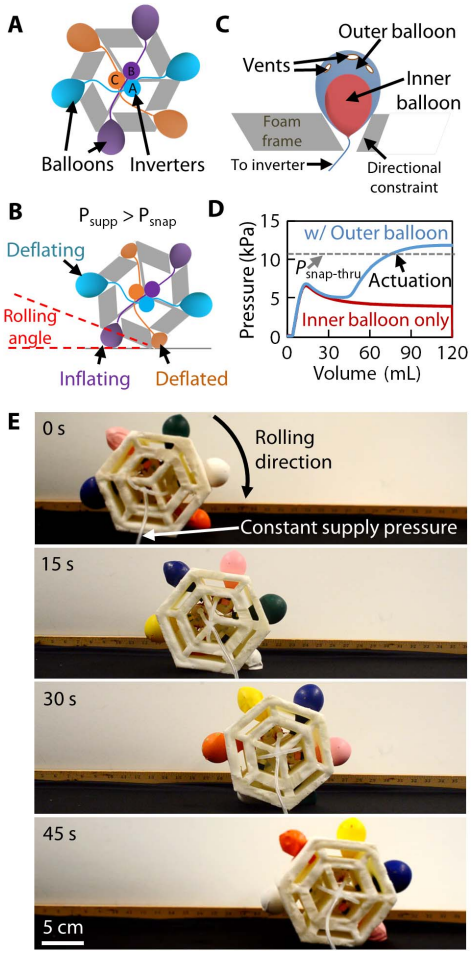

Fig. 5. Rolling soft robot driven by integrated ring oscillator. (**A**) A hexagonal roller with a soft foam frame relies on an integrated, onboard ring oscillator to inflate balloons attached to each face and to cause the hexagon to tilt as each of the balloons inflates sequentially. (**B**) Once the rolling angle reaches 30° because of inflation of a balloon, the hexagon tips onto its next face. This design uses double-balloon actuators (**C**), which exhibit a pressure-volume characteristic based on the interplay between the elastic, easy-to-stretch inner balloon and the stiff, difficult-to-stretch outer balloon (**D**). (**E**) These double-balloon actuators, mounted on each of the hexagon's six faces, cause it to tip from one face to another during inflation and roll, with only a single, constant-pressure input required. Movie S4 shows this soft robot rolling.

connections to the ring oscillator alters the direction of translation, and translation can occur along a curved or straight track (fig. S14); we show a circular track, designed and fabricated to continuously transport a ball at up to 0.012 ball lengths per second (Fig. 4, B and C), without requiring the hard components and electronic controls necessitated by previous work with a similar operating principle (*9*, *35*). In a second demonstration of motion, we integrated the ring oscillator into a completely soft, hexagonal rolling robot with a flexible foam frame. This soft robot rolls from one face of the hexagonal frame to the next as actuators attached to each face sequentially inflate and deflate (Fig. 5, A and B), in a manner similar to the design proposed by Rus and colleagues (*8*) but, in this case, without any hard components or electronic control infrastructure. To propel the rolling soft robot, we developed "double-balloon" actuators (Fig. 5C), which exhibit a unique pressure-volume characteristic (Fig. 5D): A highly extensible inner balloon can inflate indefinitely without reaching the snap-through pressure, $P_{snap\text{-}thru}$, of the inverter, but a stiffer outer balloon limits the expansion of the inner balloon and advances the ring oscillator to the next stage of oscillation by forcing the internal pressure above $P_{snap\text{-}thru}$. The balloons, attached to each face of the frame, oscillate between three states—inflating, deflating, and deflated—corresponding to the three regions of each output signal shown in Fig. 2C. When the bottom balloon inflates, the hexagon tilts, and when the rolling angle, α, exceeds 30°, the hexagon tips forward onto its next face (a face on which the balloon actuator resides in its deflated state and, therefore, does not resist the rolling motion). This deflated balloon is then inflated by the next inverter in the ring oscillator, and the rolling motion continues. We experimentally demonstrated the device, with an onboard, integrated ring oscillator, and achieved a maximum speed of 0.037 body lengths per second (Fig. 5E).

In addition to driving translational motion, the ring oscillator can control actuators for sequential or ordered manipulation in space and time; we controlled the motion of an elastomeric stage for size-based particle sorting. We created linear actuators based on the pneumatic inverter, where pressurization above the snap-through pressure, $P_{snap\text{-}thru}$, triggers actuation to an extended state, and depressurization below $P_{snap\text{-}back}$ returns the actuator to its retracted state (fig. S7, A and B). Three of these actuators, mounted axisymmetrically around the base of an elastomeric stage (fig. S7C), allow the stage to take eight positions, six of which are tilted (when either one or two of the linear actuators are extended); when these three actuators are driven by the three oscillating output pressures from the ring oscillator, the stage moves between the six tilted positions in a circularly undulating pattern. We sorted beads on the stage using a size-selective "gate" (a hole in the outer wall of the disk containing the mixed beads), with a width of the gate chosen to be between the diameters of the two beads to be sorted. The size-selective gate was placed on a wall surrounding the stage (Fig. 6A); then, when the ring oscillator repeatedly changed the stage angle by cycling the actuators, only small beads were able to escape (Fig. 6B).

The ring oscillator also enables the design of soft devices for medical or therapeutic use. Mechanotherapeutic devices—devices that apply forces or pressures to the soft tissue of the body—are a type of (often soft) actuator that can promote tissue regeneration (*36*) and represent an approach to treatment of diseases, including deep-vein thrombosis (*36*) and lymphedema resulting from venous insufficiency (*37*). We developed a textile-based mechanotherapeutic device that wraps around, and applies an upwardly propagating pressure to, the lower leg of a human user by inflating internal pneumatic chambers (Fig. 7A). Evidence indicates that sequential actuation of serially arranged pneumatic chambers extending circumferentially around the lower leg, starting from the most distal chamber to the most proximal chamber, may outperform uniform compression of the lower leg in medical applications (*38*); with this function in mind, we set out to actuate, sequentially, the internal chambers within our mechanotherapeutic device using the three output pressures of the soft ring oscillator to reduce the complexity of the required input signal while maintaining a completely soft design. Previous textile-based mechanotherapy devices have been operated at internal pressures of 29 to 86 kPa (*36*); however, the characteristic operating pressure of our soft ring oscillator, when designed as presented above, is on the order of the snap-through pressure of the inverter: 11 kPa. To actuate our fabric-based mechanotherapy device, we therefore made another soft ring oscillator using an elastomer with 3.9× higher elastic modulus

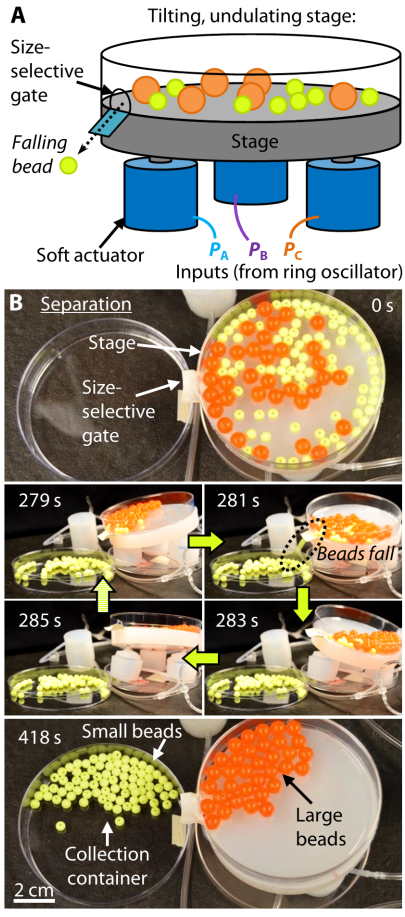

Fig. 6. Separation of particles by size. The three temporally coordinated output pressures from the ring oscillator enable separation. (**A**) When a stage is mounted on three soft linear actuators and the actuators' inputs are connected to the three pneumatic outputs of the ring oscillator (i.e., P_A, P_B, and P_C), the stage tilts in a circularly undulating pattern. (**B**) This stage motion can separate particles of different sizes when a size-selective gate is placed on the side of the stage (complete separation shown in movie S5).

(i.e., all of the Dragon Skin 10 NV components in the inverters described previously were instead fabricated using Dragon Skin 30). This ring oscillator, composed of stiffer inverters, had a higher snap-through pressure (43 kPa), within the range used to drive mechanotherapeutic devices. We attached our mechanotherapeutic device to a human user's lower leg by securing three Velcro closures (Fig. 7, B and C) and connected its inputs to the outputs of our stiffer, yet still elastomeric, Dragon Skin 30 ring oscillator. We then connected the ring oscillator to a supply pressure of P_{supp} = 50 kPa, and, using a pressure-sensitive mat (Grip Sensor, SensorEdge) directly adjacent to the user's leg (inside of the device), we measured the pressure distribution applied to the lower leg by the mechanotherapeutic device over time during operation, while the mechanotherapeutic device was being actuated by the ring oscillator. We observed alternating low- and high-pressure regions traversing up the lower leg over time (Fig. 7D), indicating that the ring oscillator inflated the chambers of the mechanotherapy device to the desired pressure (*36*) and in the desired order (*38*).

The silicone inverters used here are also compatible with many liquids and, as such, can control liquid flow when reconfigured as fluid-metering valves (fig. S16A). When the input pressure, P_{in}, to the fluid-metering valve is high ($>P_{snap\text{-}thru}$), the hemispherical membrane snaps through, unkinks the internal tubing, and allows liquid to flow (fig. S16B). When the input pressure is low ($<P_{snap\text{-}back}$), the hemispherical membrane snaps back, and flow is prevented by a kink in the buckled internal tubing (fig. S16B). We configured three fluid-metering valves to dispense blue-, red-, and green-dyed water and merged their outputs into a single channel. Then, by controlling these fluid-metering valves with the output pressures from the ring oscillator (P_A, P_B, and P_C), we generated a stream of water with periodically alternating color (figs. S16 and S17 and movie S6). In this demonstration, the three colored streams of water were pressurized with only a hydrostatic (gravitational) head at a height of 6 inches (1.5 kPa) and, nevertheless, achieved a flow rate on the order of 1 ml/s, several orders of magnitude greater than the typical liquid flow rates achieved by microfluidic devices (*21*, *39*).

DISCUSSION

Previous methods to achieve periodic, temporally coordinated actuation of multiple soft actuators have relied on hard valves operated by electrical connections, often requiring complex control systems and limiting use in applications where completely soft devices are desirable or necessary. Developments in microfluidics have demonstrated oscillatory behavior using soft materials, but with low flow rates that preclude microfluidic actuation of soft devices at larger scales. This work demonstrates a completely soft, pneumatic ring oscillator that relies on three instabilities: the buckling instability of the pneumatic tubing within the inverters, the snap-through instability of the membrane in each soft pneumatic inverter that kinks the internal tubing, and the systemic instability formed when an odd number of these inverters are connected in a ring. This soft ring oscillator generates periodic pressure signals, temporally coordinated over multiple outputs and capable of actuating macroscale devices, using only a single, constant input pressure. The ring oscillator thereby allows rotational and undulating motions in completely soft devices, exemplifying the material intelligence (i.e., the generation of "complex" behaviors achieved, primarily, through material properties) that can be leveraged through the nonlinearities of elastomeric materials.

We developed an analytical model for a ring oscillator composed of an arbitrary number of pneumatic inverters, analogous to an electronic RC circuit, which we validated against experimental results. This model allows systematic design of devices through prediction of oscillation frequency based on the supply pressure and pneumatic resistances and capacitances within the oscillator. The oscillator performance also depends on the choice of materials, shown by the increase in operating pressure (from ~15 to ~50 kPa) accompanying an increase in stiffness of the elastomers comprising the inverters (from an elastic modulus of 152 to 593 kPa, an increase of 390%). Even at its fastest, however, the soft ring oscillator only achieved frequencies approaching 1 Hz. In comparison, a pneumatic, microfluidic oscillator cycled at up to 50 Hz (*21*), and electronic ring oscillators, composed of transistors, have often achieved frequencies on the order of 10^8 to 10^{10} Hz (*32*). The present design could achieve faster frequencies through miniaturization (and a subsequent reduction in pneumatic capacitance) or through a change in design to increase the deflation speed (which limits frequency as supply pressure goes to infinity), approaching those observed in microfluidic devices. Decreasing the size of the components indirectly related to airflow, such as the internal membrane, would be particularly

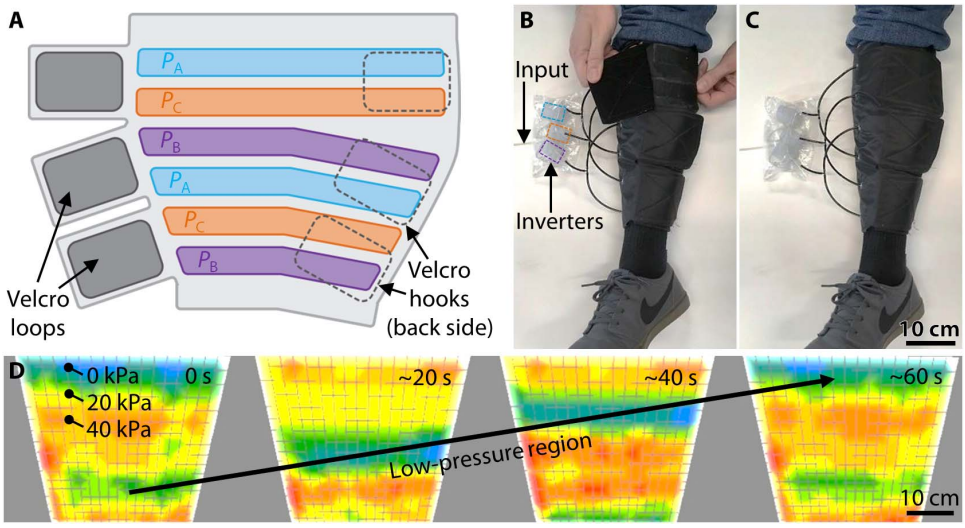

Fig. 7. Soft mechanotherapy device for the lower leg. The internal fabric chambers of the mechanotherapy device connect to the three pneumatic outputs of the ring oscillator [i.e., P_A, P_B, and P_C; (**A**)], and the device sequentially contracts around a human user's leg, "pumping" fluid up the leg for treatment of conditions such as lymphedema and chronic venous disease and for prevention of deep vein thrombosis. The device is easily applied to the lower leg with Velcro closures [top closure open (**B**); all closures closed (**C**)]. (**D**) We demonstrated propagation of a low-pressure region up the leg experimentally, using a pressure-sensitive mat placed between the mechanotherapy device and the leg; the low-pressure region corresponds to the region of fluid inside of the leg that is "pumped" upward, toward the torso (blue corresponds to a gauge pressure of 0 kPa, and red corresponds to about 50 kPa; 100 kPa ≈ 1 atm).

advantageous because high rates of airflow could be maintained. All pneumatic devices, however, face a fundamental limit—the speed of sound—that prohibits frequencies as fast as those observed in electronic oscillators, even in microscale pneumatic devices.

We used the soft ring oscillator to achieve (i) translation of spherical objects, (ii) rolling-based translational actuation of a soft robot, (iii) separation of small particles, (iv) mechanotherapy using a textile-based sleeve for the lower leg, and (v) fluid metering—all with entirely soft components. When combined with a portable source of pressurized air at constant pressure (such as a cylinder of compressed air, a gas-generating chemical reaction, or a thermally driven vaporizing liquid), the ring oscillator could enable these applications and others requiring temporally coordinated actuation of multiple components, in remote environments, and without the need for supporting infrastructure. The ring oscillator could, e.g., drive motion, or other functions, of truly "untethered" and completely soft robots that do not rely on external pneumatic or electronic connections for power. This functionality may be particularly useful in high radiative fields resulting, e.g., from nuclear accidents or contamination [albeit pending further development in soft autonomous control (*40*)]. A soft rolling robot based on the ring oscillator could presumably travel into a high-radiation environment, take measurements or samples, and then return the collected data to a human user.

Fabrication of the inverters comprising the ring oscillator remains difficult to achieve with modern advanced manufacturing techniques; the inverters are cast in three-dimensional (3D)–printed molds, and several elastomeric pieces must then be assembled manually. The manufacturing process could be simplified by direct 3D printing, or potentially even roll-to-roll processing of a 2D version, of the elastomeric inverters used in this work. Despite present challenges in fabrication, however, the relatively low cost (*3*), high cycle lifetime (up to millions of cycles) (*5*, *6*), and, for biological applications, ease of sterilization (*4*) of soft devices make them an attractive alternative to hard, mechanical systems that require electronic controls to achieve the same functionality. This soft ring oscillator eliminates the need for an electronic control infrastructure in these applications and allows implementation in areas where hard components or electronics are not compatible, including underwater; in vivo; in the presence of high magnetic, electric, or radiative fields; or in applications where actuators may experience substantial bending, compressive, or tensile stresses.

MATERIALS AND METHODS

Research objectives and design

This study was designed to experimentally demonstrate the soft ring oscillator, with parametric sweeps performed over the relevant system parameters (supply pressure, pneumatic resistance, and pneumatic capacitance) for validation of the analytical model developed in this work. We also demonstrated several prototypical applications driven by the output pressures of the soft ring oscillator, each implemented without hard components, to highlight that the ring oscillator can be integrated into completely soft devices to generate complex motions and behaviors using only one input at a constant pressure. We fabricated all of the components of the ring oscillator and the soft devices for the prototypical applications from commercially available, inexpensive materials to reduce barriers to reproduction of our work.

Fabrication of elastomeric components

We used three different commercially available elastomers manufactured by Smooth-On: Dragon Skin 10 NV (semitransparent), Dragon Skin 30 (semitransparent), and Smooth-Sil 950 (blue). Their prepolymer mixtures were prepared in three steps: (i) adding the two components, "A" and "B," (ii) mixing the components by manually stirring them, and (iii) degassing the mixture under vacuum. The prepolymer mixtures of Dragon Skin 10 NV and Dragon Skin 30 were prepared by mixing the two components in a ratio of 1:1, stirring the mixture manually for ~2 min, and degassing for ~5 min in a vacuum dessicator. The prepolymer mixture of Smooth-Sil 950 was prepared by mixing its components in a ratio of 10:1, stirring the mixture for ~5 min, and degassing for ~10 min. The degassed prepolymer elastomers were poured into 3D-printed molds and cured to create the components of all of the soft devices, including the inverters, used in this work. Details specific to the fabrication of each device, along with schematics of the molds and assembly diagrams when multiple components were used, are presented in the Supplementary Materials.

Fabrication of the textile-based mechanotherapy device

A stretchable, heat-sealable knit fabric (Dri-Tek 8020, Eastex Products Inc.) and an inextensible, heat-sealable woven fabric (Heat Sealable 70 Denier Coated Nylon Taffeta, Seattle Fabrics) were cut to a patterned

size with a 60-W CO_2 laser (VLS6.60, Universal Laser Systems) set to 100% speed, 55% power, and 1000 pulses per inch. The inextensible fabric pattern included 1-mm through-holes for tubing. M2 vented screws were placed through the holes, secured with nuts, and attached to external tubing. Teflon sheets (PTFE Teflon Sheet, SS SHOVAN) were manually cut to the internal chamber sizes and placed between the heat-sealable fabric layers. The full layup was bonded with heat and pressure in a pneumatic heat press (DK20SP, Geo Knight & Co. Inc.) at settings of 170°C and 413 kPa for 30 s. A hook fastener (Velcro) was attached with instant adhesive on top of the chambers, and a loop fastener (Velcro) was machine-sewn in place at the tabs.

Characterization of a soft, pneumatic inverter

A single soft, pneumatic inverter was tested in the experimental configuration shown in fig. S10 to generate the data in figs. S11 and S12. We varied input pressure with a voltage-controlled pressure regulator (ITV0010-2BL, SMC Pneumatics) interfaced to a computer and characterized and recorded input, output, and supply pressures with electronic pressure sensors (ADP5151, Panasonic) connected to a data acquisition system (NI USB-6218 BNC). The supply pressure was set with a manual pressure regulator (Watts 03904). The input pressure was increased linearly from 0 to 20 kPa over 60 s and then decreased linearly back to 0 kPa over 60 s.

Characterization of the soft ring oscillator

During operation of the ring oscillator, three electronic pressure sensors (ADP5151, Panasonic) were attached to the connections between each of the inverters to measure the output pressures P_A, P_B, and P_C. The supply pressure, P_{supp}, which was regulated by a manual pressure regulator (Watts 03904), was measured with a fourth electronic pressure sensor of the same type (ADP5151, Panasonic).

SUPPLEMENTARY MATERIALS

robotics.sciencemag.org/cgi/content/full/4/31/eaaw5496/DC1
Materials and Methods
Text
Fig. S1. Design of the molds for the tubing used inside the chambers of the inverter.
Fig. S2. Assembly of the tubing used inside the chambers of the inverter.
Fig. S3. Design of the molds for the inverter.
Fig. S4. Assembly of the inverter.
Fig. S5. Design of the molds, and assembly, for the ball roller (circular track).
Fig. S6. Design of the molds, and assembly, for the rolling hexagonal frame.
Fig. S7. Design and assembly of the soft, undulating stage.
Fig. S8. Unactuated and actuated inverter schematics, with labels, alongside photographs.
Fig. S9. Membrane snap-through hysteresis.
Fig. S10. Experimental setup for characterization of the soft, pneumatic inverter.
Fig. S11. Inverting Schmitt trigger–like behavior.
Fig. S12. P_{supp} does not influence the critical pressures.
Fig. S13. Pneumatic RC circuit analog.
Fig. S14. A soft linear ball roller connected to the ring oscillator.
Fig. S15. Soft stage mounted on three linear actuators connected to the ring oscillator.
Fig. S16. The soft ring oscillator can control and meter fluid flows.
Fig. S17. Experimental setup for the demonstration of metering of fluid.
Data file S1. Zip file containing stereolithography (STL) files of 3D-printed molds used in this work.
Movie S1. Single inverter demonstration: When the input is off (0), the output is on (1), and vice versa.
Movie S2. High-strain deformation test: The ring oscillator is manually compressed to 25% of its initial size, after which it resumes operation.
Movie S3. Translation of spherical object around a circular elastomeric track.
Movie S4. Actuation of a rolling soft robot with an integrated soft ring oscillator.
Movie S5. Separation using an elastomeric stage driven by the soft ring oscillator.
Movie S6. Fluid-metering valves controlled by the soft ring oscillator.
Reference (*41*)

REFERENCES AND NOTES

1. G. M. Whitesides, Soft robotics. *Angew Chem. Int. Ed.* **57**, 4258–4273 (2018).
2. D. Rus, M. T. Tolley, Design, fabrication and control of soft robots. *Nature* **521**, 467–475 (2015).
3. P. Polygerinos, N. Correll, S. A. Morin, B. Mosadegh, C. D. Onal, K. Petersen, M. Cianchetti, M. T. Tolley, R. F. Shepherd, Soft robotics: Review of fluid-driven intrinsically soft devices; manufacturing, sensing, control, and applications in human-robot interaction. *Adv. Eng. Mater.* **19**, 1700016 (2017).
4. A. De Greef, P. Lambert, A. Delchambre, Towards flexible medical instruments: Review of flexible fluidic actuators. *Precis. Eng.* **33**, 311–321 (2009).
5. P. Rothemund, A. Ainla, L. Belding, D. J. Preston, S. Kurihara, Z. Suo, G. M. Whitesides, A soft, bistable valve for autonomous control of soft actuators. *Sci. Robot.* **3**, 7986 (2018).
6. D. Yang, M. S. Verma, J.-H. So, B. Mosadegh, C. Keplinger, B. Lee, F. Khashai, E. Lossner, Z. G. Suo, G. M. Whitesides, Buckling pneumatic linear actuators inspired by muscle. *Adv. Mater. Technol.* **1**, 1600055 (2016).
7. B. Mosadegh, P. Polygerinos, C. Keplinger, S. Wennstedt, R. F. Shepherd, U. Gupta, J. Shim, K. Bertoldi, C. J. Walsh, G. M. Whitesides, Pneumatic networks for soft robotics that actuate rapidly. *Adv. Funct. Mater.* **24**, 2163–2170 (2014).
8. A. D. Marchese, C. D. Onal, D. Rus, Soft robots actuators using energy-efficient valves controlled by electropermanent magnets, in *IEEE/RSJ International Conference on Intelligent Robots and Systems* (IEEE, 2011), pp. 756–761.
9. B. Mosadegh, A. D. Mazzeo, R. F. Shepherd, S. A. Morin, U. Gupta, I. Z. Sani, D. Lai, S. Takayama, G. M. Whitesides, Control of soft machines using actuators operated by a braille display. *Lab Chip* **14**, 189–199 (2014).
10. F. Esser, T. Steger, D. Bach, T. Masselter, T. Speck, Development of novel foam-based soft robotic ring actuators for a biomimetic peristaltic pumping system, in *Conference on Biomimetic and Biohybrid Systems* (Springer, 2017), pp. 138–147.
11. S. Dirven, M. Stommel, R. Hashem, W. Xu, Medically-inspired appraoches for the analysis of soft-robotic motion control, in *IEEE 14th International Workshop on Advanced Motion Control* (IEEE, 2016), pp. 370–375.
12. S. Dirven, F. J. Chen, W. L. Xu, J. E. Bronlund, J. Allen, L. K. Cheng, Design and characterization of a peristaltic actuator inspired by esophageal swallowing, in *IEEE/ASME Transactions on Mechatronics* (IEEE, 2014), vol. 19, pp. 1234–1242.
13. M. T. Tolley, R. F. Shepherd, B. Mosadegh, K. C. Galloway, M. Wehner, M. Karpelson, R. J. Wood, G. M. Whitesides, A resilient, untethered soft robot. *Soft Robot* **1**, 213–223 (2014).
14. R. K. Katzschmann, A. de Maille, D. L. Dorhout, D. Rus, Cyclic hydraulic actuation for soft robotic devices, in *IEEE/RSJ International Conference on Intelligent Robots and Systems* (IEEE, 2016), pp. 3048–3055.
15. N. Correll, Ç. D. Önal, H. Liang, E. Schoenfeld, D. Rus, Soft autonomous materials—Using active elasticity and embedded distributed computation, in *Experimental Robotics* (Springer, Berlin, 2014), pp. 227–240.
16. R. F. Shepherd, A. A. Stokes, J. Freake, J. Barber, P. W. Snyder, A. D. Mazzeo, L. Cademartiri, S. A. Morin, G. M. Whitesides, Using explosions to power a soft robot. *Angew Chem. Int. Ed.* **52**, 2892–2896 (2013).
17. M. Wehner, R. L. Truby, D. J. Fitzgerald, B. Mosadegh, G. M. Whitesides, J. A. Lewis, R. J. Wood, An integrated design and fabrication strategy for entirely soft, autonomous robots. *Nature* **536**, 451–455 (2016).
18. N. Vasios, A. J. Gross, S. Soifer, J. T. B. Overvelde, K. Bertoldi, Harnessing viscous flow to simplify the actuation of fluidic soft robots. *Soft Robot* 10.1089/soro.2018.0149 (2019).
19. B. Gorissen, E. Milana, A. Baeyens, E. Broeders, J. Christiaens, K. Collin, D. Reynaerts, M. De Volder, Hardware sequencing of inflatable nonlinear actuators for autonomous soft robots. *Adv. Mater.* **31**, e1804598 (2019).
20. Q. D. Zhang, M. Zhang, L. Djeghlaf, J. Bataille, J. Gamby, A. M. Haghiri-Gosnet, A. Pallandre, Logic digital fluidic in miniaturized functional devices: Perspective to the next generation of microfluidic lab-on-chips. *Electrophoresis* **38**, 953–976 (2017).
21. P. N. Duncan, T. V. Nguyen, E. E. Hui, Pneumatic oscillator circuits for timing and control of integrated microfluidics. *Proc. Natl. Acad. Sci. U.S.A.* **110**, 18104–18109 (2013).
22. P. N. Duncan, S. Ahrar, E. E. Hui, Scaling of pneumatic digital logic circuits. *Lab Chip* **15**, 1360–1365 (2015).
23. S. Ahrar, P. N. Duncan, E. E. Hui, Programmable microfluidic digital logic for the autonomous lab on a chip, in *18th International Conference On Miniaturized Systems For Chemistry and Life Sciences* (Chemical and Biological Microsystems Society, 2014), pp. 1512–1514.
24. T. V. Nguyen, P. N. Duncan, S. Ahrar, E. E. Hui, Semi-autonomous liquid handling via on-chip pneumatic digital logic. *Lab Chip* **12**, 3991–3994 (2012).
25. M. A. Unger, H.-P. Chou, T. Thorsen, A. Scherer, S. R. Quake, Monolithic microfabricated valves and pumps by multilayer soft lithography. *Science* **288**, 113–116 (2000).
26. K. Hosokawa, R. Maeda, A pneumatically-actuated three-way microvalve fabricated with polydimethylsiloxane using the membrane transfer technique. *J. Micromech. Microeng.* **10**, 415–420 (2000).

27. E. C. Jensen, W. H. Grover, R. A. Mathies, Micropneumatic digital logic structures for integrated microdevice computation and control. *J. Microelectromech. Syst.* **16**, 1378–1385 (2007).
28. W. H. Grover, R. H. C. Ivester, E. C. Jensen, R. A. Mathies, Development and multiplexed control of latching pneumatic valves using microfluidic logical structures. *Lab Chip* **6**, 623–631 (2006).
29. B. Mosadegh, C. H. Kuo, Y. C. Tung, Y. S. Torisawa, T. Bersano-Begey, H. Tavana, S. Takayama, Integrated elastomeric components for autonomous regulation of sequential and oscillatory flow switching in microfluidic devices. *Nat. Phys.* **6**, 433–437 (2010).
30. E.-F. M. Henke, S. Schlatter, I. A. Anderson, Soft dielectric elastomer oscillators driving bioinspired robots. *Soft Robot.* **4**, 353–366 (2017).
31. B. M. O'Brien, I. A. Anderson, An Artificial Muscle Ring Oscillator, in *IEEE - ASME Transactions on Mechatronics* (IEEE, 2012), pp. 197–200.
32. P. Horowitz, W. Hill, *The Art of Electronics* (Cambridge Univ. Press, Cambridge England, New York, ed. 2, 1989), pp. 1125.
33. Y. Sasaki, K. Namba, H. Ito, Soft error masking circuit and latch using Schmitt trigger circuit, in *Proceedings of 21st IEEE International Symposium on Defect and Fault-Tolerance in VLSI Systems* (IEEE, 2006), pp. 327–335.
34. A. Pandey, D. E. Moulton, D. Vella, D. P. Holmes, Dynamics of snapping beams and jumping poppers. *Europhys. Lett.* **105**, 24001 (2014).
35. X. Y. Gong, K. Yang, J. J. Xie, Y. J. Wang, P. Kulkarni, A. S. Hobbs, A. D. Mazzeo, Rotary actuators based on pneumatically driven elastomeric structures. *Adv. Mater.* **28**, 7533–7538 (2016).
36. C. J. Payne, E. G. Hevia, N. Phipps, A. Atalay, O. Atalay, B. R. Seo, D. J. Mooney, C. J. Walsh, Force control of textile-based soft wearable robots for mechanotherapy, in *IEEE International Conference on Robotics and Automation (ICRA)*, Brisbane, Australia, 21 to 25 May 2018, pp. 5459–5465.
37. M. T. Loghmani, M. Whitted, Soft tissue manipulation: A powerful form of mechanotherapy. *J. Physiother. Phys. Rehabil.* **1**, 122 (2016).
38. R. J. Morris, J. P. Woodcock, Evidence-based compression: Prevention of stasis and deep vein thrombosis. *Ann. Surg.* **239**, 162–171 (2004).
39. N. Pamme, Continuous flow separations in microfluidic devices. *Lab Chip* **7**, 1644–1659 (2007).
40. D. J. Preston, P. Rothemund, H. J. Jiang, M. P. Nemitz, J. Rawson, Z. G. Suo, G. M. Whitesides, Digital logic for soft devices. *Proc. Natl. Acad. Sci. U.S.A.* **116**, 7750–7759 (2019).
41. C. T. Crowe, *Engineering Fluid Mechanics* (John Wiley & Sons, Hoboken, NJ, ed. 9, 2009).

Funding: This research was partly funded by an award from the Department of Energy (DOE), Office of Basic Energy Science, Division of Materials Science and Engineering under award ER45852, which funded all work related to experimental apparatus and demonstrations. We also acknowledge National Science Foundation (NSF) award no. IIS-11317744 for some supplies and NSF MRSEC award DMR-1420570 for partial salary support and access to shared facilities. H.J.J. acknowledges the support of the Harvard Mobility Scheme, The University of Sydney, Australia. V.S. acknowledges the support of the U.S. Department of Defense through the National Defense Science and Engineering Graduate (NDSEG) Fellowship Program and the National GEM Consortium through the GEM Fellowship. **Author contributions:** D.J.P., P.R., and G.M.W. conceived the work. D.J.P., H.J.J., V.S., J.R., and W.-K.L. fabricated the devices. All authors contributed to the experimental setup and the collection and interpretation of data. D.J.P. and P.R. developed the analytical model. D.J.P. and G.M.W. oversaw the work. **Competing interests:** G.M.W. acknowledges an equity interest and board position in Soft Robotics Inc. All other authors declare that they have no competing interests. **Data and materials availability:** All data needed to evaluate the conclusions in the paper are present in the paper or the Supplementary Materials.

Submitted 4 January 2019
Accepted 27 May 2019
Published 26 June 2019
10.1126/scirobotics.aaw5496

Citation: D. J. Preston, H. J. Jiang, V. Sanchez, P. Rothemund, J. Rawson, M. P. Nemitz, W.-K. Lee, Z. Suo, C. J. Walsh, G. M. Whitesides, A soft ring oscillator. *Sci. Robot.* **4**, eaaw5496 (2019).

A soft ring oscillator

Daniel J. Preston, Haihui Joy Jiang, Vanessa Sanchez, Philipp Rothemund, Jeff Rawson, Markus P. Nemitz, Won-Kyu Lee, Zhigang Suo, Conor J. Walsh and George M. Whitesides

Sci. Robotics **4**, eaaw5496.
DOI: 10.1126/scirobotics.aaw5496